ACS Combinatorial Science

Research Article

pubs.acs.org/acscombsci

Combinatorial Development of Novel Pd Based Mixed Oxide Catalysts for the CO Hydrogenation to Methanol

M. Reiser, K. Stöwe, and W. F. Maier*

Lehrstuhl für Technische Chemie, Universität des Saarlandes, Gebäude C 4.2, 66123 Saarbrücken, Germany

ABSTRACT: In a combinatorial study numerous palladium containing mixed oxides were synthesized by a sol−gel approach and screened for their catalytic activity toward methanol synthesis from synthesis gas. Several materials exhibited higher yields than comparable supported catalysts. Titanium based materials showed to be the most promising catalytic materials, which exhibited good selectivities for temperatures below 265 °C. The materials investigated are characterized by high specific surface areas and high pore volumes which seem to have a beneficial effect on the reactivity.

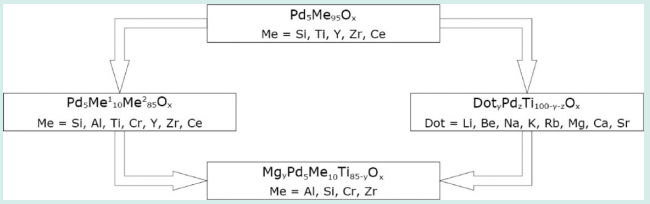

KEYWORDS: *methanol synthesis, Pd-catalysts, combinatorial catalysis, synthesis gas, heterogeneous catalysis*

1. INTRODUCTION

With a production volume of 42 million tons in 2009, methanol is one of the key feedstocks for the chemical industry.[1,2] Because of its high energy density, methanol is also considered to be an attractive alternative as energy carrier and fuel, as well as feedstock for a future economy based on methanol.[3] In the context of a sustainable "methanol economy", the production of methanol from renewable feedstocks, such as biomass, appears to be an attractive option. On an industrial scale methanol is prepared from synthesis gas at elevated pressures and temperatures using Cu−Zn based catalysts. These catalyst systems are highly sophisticated and are characterized by large space time yields together with selectivities beyond 99%.[4] One major drawback of Cu catalysts is their inferior tolerance toward catalyst poisons such as sulfur or chlorine. In view of the use of biomass as feedstock for methanol synthesis, costly workup procedures would be necessary prior to methanol synthesis since biomass can contain significant amounts of sulfur[5] and other catalyst poisons. A less considered class of catalysts are palladium based. In their pioneering work Poutsma et al. demonstrated that methanol could be produced from carbon monoxide and hydrogen over supported palladium with high selectivities at elevated pressures.[6] Subsequent studies showed that activity and product selectivity of carbon monoxide hydrogenation is strongly dependent on the support material. Ryndin et al. studied the reactivity of highly dispersed Pd on different supports.[7] At 250 °C and 10 atm they report the following order of reactivity: $ZrO_2 > La_2O_3 > ZnO > TiO_2 > MgO \approx Al_2O_3 \approx SiO_2$. Methanol yield did not correlate directly with CO hydrogenation activity, so another order was observed for methanol selectivity: $ZnO > La_2O_3 > MgO \approx SiO_2 \gg ZrO_2 \gg TiO_2 > Al_2O_3$. While SiO_2 exhibited a selectivity above 90%, the much lower selectivities of ZrO_2 and TiO_2 of 42% and 22%, respectively, were attributed to the acidity of the supports. These results were supported by studies of Fajula et al., who showed that the methanation activity of Pd/SiO_2 increases with the acidity of the SiO_2 support.[8] Methanol synthesis, on the other hand, was essentially influenced by small Pd crystallites on which methanol formation was favored because of weaker CO adsorption relative to large crystallites. Shen and Matsumura investigated the interactions between Pd and various supports (SiO_2, Al_2O_3, TiO_2, ZrO_2) and their influences on activity and selectivity.[9] As the test conditions (20 bar, 200−300 °C) differed from those used by Ryndin et al.,[7] a different order of reactivity was observed. At 200 °C all catalysts except for Pd/Al_2O_3 showed methanol selectivities above 90%, while for Pd/TiO_2 methanation became the dominant reaction above 250 °C. For Pd/ZrO_2, which was both highly active and selective, strong metal support interactions (SMSI) were observed, which resulted in the formation of cationic Pd species at the interface of support and metal. As these results were in agreement with the findings by Ponec,[10,11] they concluded that Pd^+ species are favorable for methanol synthesis. Albeit SMSI have a promoting effect on activity and selectivity, their presence is no prerequisite for the catalytic effect of Pd.[12] Today it is generally accepted that the dissociation of H_2 takes place on Pd^0, while CO is hydrogenated on cationic Pd or at active centers on the support.[13−16] Among the supported Pd catalysts Pd/CeO_2 is characterized by extraordinary methanol space time yields together with high selectivities.[17,18] Because CeO_2 is easily reduced, the SMSI effects are remarkably strong.[19] Another interesting property is the tolerance of Pd/CeO_2 against H_2S up to concentrations of 30 ppm in the reaction gas mixture.[20] CeO_2 acts as a sulfur sink, as the formation of Ce_2O_2S is favored over the formation of PdS under reductive conditions.

The aim of this work was to develop or identify new Pd containing mixed oxides with improved catalytic properties for

Received: November 10, 2011
Revised: March 16, 2012
Published: May 4, 2012

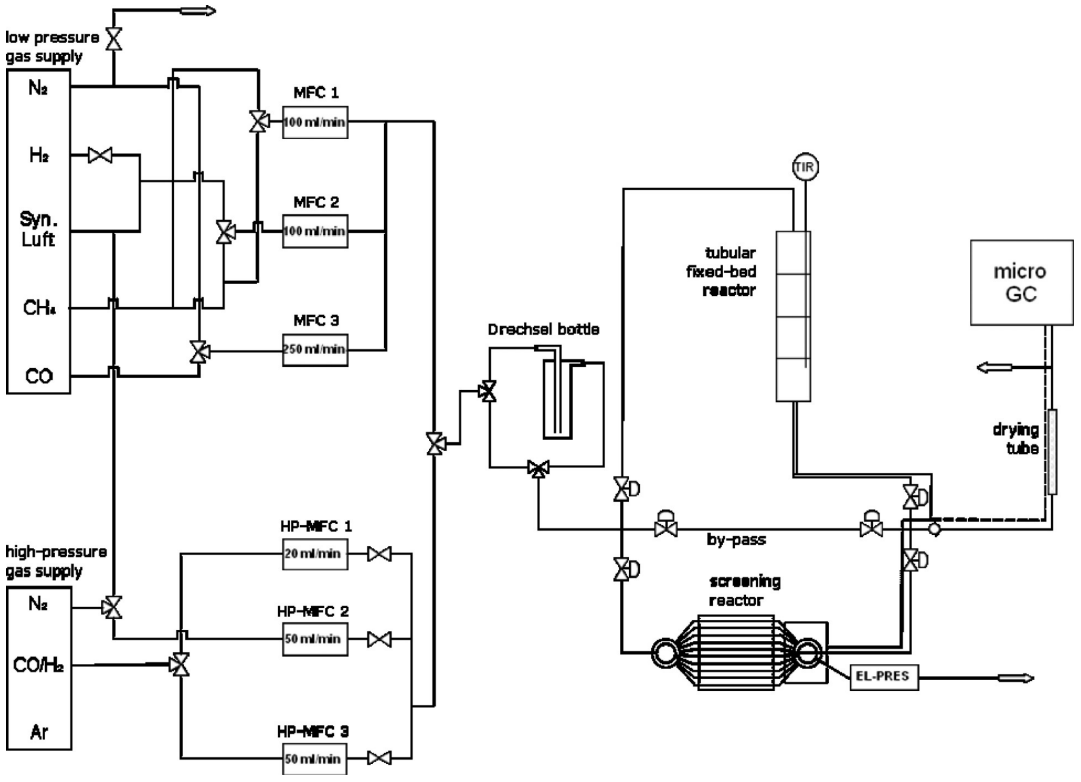

Figure 1. Flow scheme of the test setup.

the methanol synthesis from synthesis gas using high-throughput experimentation for an accelerated testing of catalytic properties.[21] For materials synthesis the sol−gel process was applied, which allows the preparation of porous, homogeneous mixed oxides for a wide variety of element combinations and compositions under mild conditions.[22] The combinatorial development was based on known supported catalysts. The analogous mixed oxides were prepared by an acid catalyzed sol−gel synthesis route and modified by combination and doping. For the screening a pressurized microreactor was used.

2. EXPERIMENTAL PROCEDURES

A simplified notation is used to name the materials: the composition of a binary mixed oxide (O_x) is generally described as $A_aB_bO_x$. A and B denote a particular element, the lower case *a* and *b* describe the molar fraction of the respective element in mol% (with $a + b = 100$ mol%) not accounting for the oxidation states of the elements in the compound and thus not for any oxide content, since this may vary depending on treatments and environment. Consequently, the mixture may be either metallic or oxidic or a mixture of both.

2.1. Catalysts Synthesis. All catalysts were synthesized following a modified sol−gel process which was developed by D. K. Kim in our group.[23] For the synthesis of 5 mmol of $Pd_5Ti_{95}O_x$ 3.7 mL of 4-hydroxy-4-methyl-2-pentanone (30 mmol) were placed in a glass beaker. Subsequently, 4.75 mL of 1 M titanium tetraisopropoxide in acetone and 2.5 mL of 0.1 M palladium acetate in acetone were added under stirring. Then the beaker was sealed with sealing tape, and the solution was stirred for 30 min before adding 15 μL of propionic acid (0.2 mmol). After 2 h of stirring the sealing tape was partly removed, and the mixture was dried for 5 days at room temperature, followed by 2 d at 40 °C. The dried gel was calcined in air at 300 °C for 5 h (heating ramp: 12 °C/h).

2.2. Catalyst Test Setup. The test equipment included a microreactor for the catalyst screening, a tubular fixed bed reactor for catalyst testing under conventional conditions, and a bypass. Gas was supplied by 2 groups of mass flow controllers for low pressure and high pressure operations, respectively. The setup was controlled by the process control system MSR_Manager (Software MENUE, both by HiTec Zang). Pressure regulation was done by means of a relief valve whose opening pressure could be varied between 5 and 100 bar. The effluent gases were analyzed by means of a microgas chromatograph (Varian CP4900) which was equipped with two columns. A 5 Å molsieve column (CP-Molsieve 5A) was used to separate and quantify H_2, CO, and CH_4. Light hydrocarbons ($<C_5$) were separated by a dimethylpolysiloxane column (CP-Sil 5CB), whereas only methanol was quantified. The lines from the reactor outlets to the gas chromatograph were heated to avoid the condensation of methanol or other liquid reaction products inside the capillary. Additionally the effluent gas was dried by means of a stainless steel tube filled with the desiccant Drierite ($CaSO_4/CoCl_2$; grain size 1−2 mm). In Figure.1 the flow scheme of the setup is given.

High-Throughput Screening. For the sequential screening of catalysts libraries a pressurized 10-channel microreactor was used. The reactor consisted of a large mass stainless steel body inside of which was placed a stack of 10 microstructured platelets. In Figure 2 and 3 the microreactor is shown while the platelets are shown in Figure 4. The platelets, having a length of 50 mm and a width of 5 mm, possessed 12 etched microchannels (0.5−0.6 mm diameter) into which the catalyst powders were coated. Thereto 15 mg of catalyst with particle sizes between 50−100 μm were added to 150 μL of a mixture of 5.8 wt % polyvinyl alcohol in water and stirred to disperse

dx.doi.org/10.1021/co200191a | ACS Comb. Sci. 2012, 14, 378−387

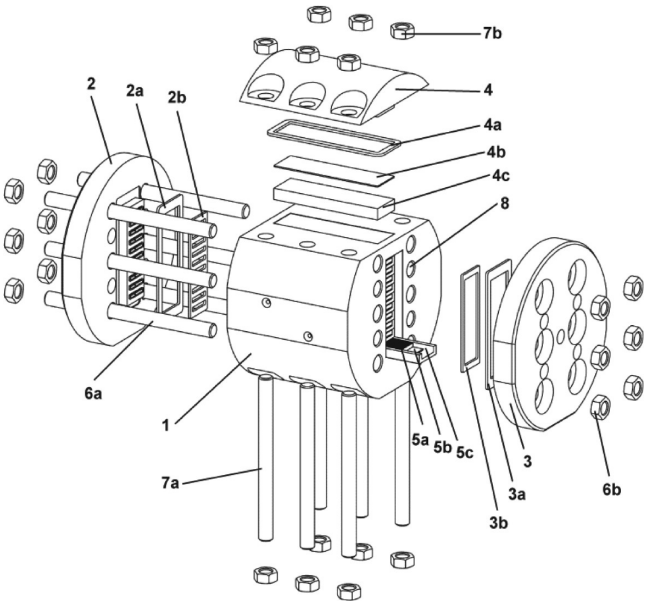

Figure 2. Exploded view of the microreactor (IMM GmbH). 1 reactor chamber; 2 parallel outlet; 2a/b graphite gaskets; 3 parallel inlet; 3a/b graphite gaskets; 4 top cover; 4a graphite gasket; 4b adjustment body; 4c pressure plate; 5a plate drawer; 5b graphite gasket; 5c microplatelet; 6a/b radial screws 7a/b axial screws; 8 bore holes for heating cartridges.

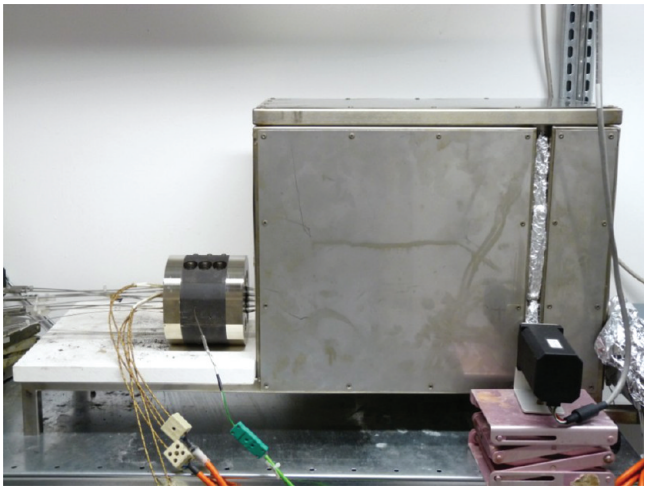

Figure 3. Representation of the microreactor with the valve heating box.

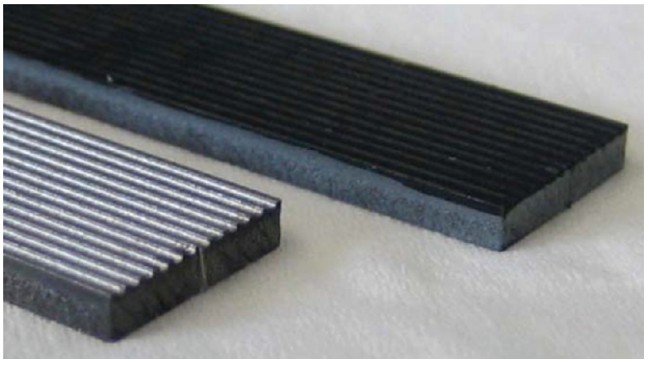

Figure 4. Uncoated and coated microstructured platelet.

the particles. One hundred microliters of the suspension were transferred onto the platelet, and excess suspension was wiped off with a razor blade. The coated platelets were dried for 10 h at 105 °C (heating ramp: 10 °C/h) and subsequently calcined for 5 h at 300 °C (heating ramp: 10 °C/h). The coated platelets were weighed after calcination. All 10 individual platelets were mounted in the reactor.

In a typical screening experiment up to 8 catalysts together with a reference catalyst and one uncoated platelet were tested. As reference catalyst an industrial $Cu/ZnO/Al_2O_3$ catalyst was used throughout this study. For each experiment the positions of the samples were chosen arbitrarily. The inlet and the outlet of the reactor were attached to 10-port multiposition valves, which allowed for the switching between channels. Prior to the screening experiment the catalysts were activated for 1 h at 265 °C and 30 bar in a flow of 15 mL/min of the reaction gas mixture (33 vol % CO balanced with H_2). The catalysts were screened sequentially at 235 °C and 30 bar with a flow of the reaction mixture of 12 mL/min for 4.5 h respectively.

Conventional Catalyst Testing. Conventional catalytic tests were carried out in a pressurized tubular fixed-bed reactor. Fresh catalyst samples (100 mg, 50−100 μm) were diluted with 400 mg quartz sand (100−200 μm). The diluted sample was placed on a glass frit inside a glass tube, which was inserted into the stainless steel jacket of the reactor. Inlet and outlet of the reactor were sealed by means of flanges. After reductive pretreatment in 50 vol % H_2 balanced with N_2 for 1 h at 300 °C at ambient pressure, the reactant gas mixture (33 vol % CO balanced with H_2) was fed to the reactor at a flow rate of 12 mL/min at bed temperatures between 200 and 300 °C. The pressure of 30 bar was maintained by means of an adjustable relief valve placed at the exit of the reactor. At the beginning and the end of each catalytic test the gas mixture was passed through the bypass. The effluent gas was analyzed by means of the same microgas chromatograph as used in the high-throughput screening.

2.3. Catalyst Characterization. Specific surface areas were determined by static volumetric physisorption with nitrogen at 77.3 K or with Argon at 87.5 K by means of a Sorptomatic 1990 (Carlo Erba). Prior to the adsorption experiments the samples were outgassed under vacuum for 2 h at 200 °C. The specific surface areas were calculated according to the theory of Brunauer, Emmett, and Teller;[24,25] for the analysis of the distribution of mesopores the method of Barrett, Joyner, and Halenda was used.[26]

The powder X-ray diffraction patterns were collected using a PANalytical X'Pert diffractometer in θ/θ−geometry equipped with a PIXcel detector using Ni filtered Cu radiation. For the evaluation of the diffraction patterns X'Pert HighScore Plus software was used.[27] The phases were assigned using the ICSD database. The refining of the crystal structure parameters and of the particle size was carried out with the program TOPAS using a fundamental parameter approach.[28]

Transmission electron microscopy (TEM) images were recorded by means of a JEM 2001 transmission electron microscope (JEOL).

3. RESULTS AND DISCUSSION

3.1. Combinatorial Search. The process of catalyst development can be significantly accelerated by implementing high-throughput and combinatorial techniques. As the search space of elemental combinations is of nearly infinite dimensions, a suitable search strategy is indispensable for a

successful screening for new catalyst formations. There are basically two approaches.[31] In the knowledge based approach elements and element combinations are chosen based on chemical knowledge about the catalytic properties of the chosen elements for a given reaction. In this case the search space is limited to finite number of elements, and the goal of the combinatorial development is essentially the improvement of known catalyst systems. The second approach is based on a more or less random combination of elements.

In preceding studies a broad screening with a highly diverse collection of mixed oxides did not lead to any promising discovery.[29,30] Because of the limited throughput of the screening setup presented here, the knowledge based approach is applied in this study. Supported Pd catalysts are known to be selective for the methanol synthesis from CO and H_2 where the intimate contact between metal and support seems to be favorable. The acid catalyzed sol−gel process allows for the preparation of oxides mixed on an atomic scale[22] and hence an optimal contact between metal and "support" can be achieved. Because of the intimate mixing of sol−gel materials, differences in activity and selectivity of the catalysts relative to conventionally prepared materials (e.g., by impregnation) can be expected.

The starting point of the combinatorial search was a group of base metals which form typical support oxides for catalysts. In a first step these metals were combined with Pd and further varied throughout the generations.

Results of Generation 1. In the first generation, binary oxides consisting of 5 mol% Pd and a second metal oxide were prepared. The aim of this generation was to identify promising elements which were suitable as matrix elements on the way toward novel Pd based methanol synthesis catalysts. The elements were chosen on the basis of known supported catalysts, which were described as active catalysts for methanol synthesis. Pd/CeO_2 and Pd/ZrO_2 show both high activities and selectivites.[9,17,18] Pd/SiO_2 and Pd/TiO_2 were characterized by either a high selectivity together with a low activity or by a high activity but a low selectivity, respectively.[7,9] Additionally Y_2O_3 was chosen as support as it is known to exhibit strong metal support interactions (SMSI) with Pd, which are believed to be beneficial for the methanol synthesis activity of supported Pd catalysts.[32] No other metals were chosen since they either dissociate CO upon adsorption (Fe, Co, Ni[33,34]) or were not accessible to synthesis with the sol-gel method applied here (Cr, Mn, Zn, Mo). Because of the small number of catalysts, all materials were tested in the conventional fixed bed reactor.

The results of the catalytic tests are depicted in Figure 5. The by far highest space time yield of methanol was observed for $Pd_5Ti_{95}O_x$, while $Pd_5Y_{95}O_x$ and $Pd_5Ce_{95}O_x$ showed only moderate methanol yields. For $Pd_5Si_{95}O_x$ and $Pd_5Zr_{95}O_x$ only negligible methanol yields were observed. Besides $Pd_5Zr_{95}O_x$, which appeared to be completely inactive for methanol synthesis, the observed reactivity order was in agreement with results from the literature.[7,9] The catalysts showed large differences in their selectivity. Besides methanol, methane, and ethane no other byproducts were detected by gas chromatography (GC), which allowed for analysis of organic compounds up to C_5. In general, the methanation rate increased with temperature and became the dominant reaction at high temperatures. For $Pd_5Ti_{95}O_x$ the methanol yield decreased drastically above a temperature of 235 °C, while the methane yield surpasses the methanol yield at 265 °C. These findings were in good agreement with the results of Shen et al. who found a similar behavior for Pd/TiO_2 in methanol synthesis with CO_2 free syngas.[9] For $Pd_5Ce_{95}O_x$ the methane yield was always comparable to or larger than that of methanol which was surprising as the methanation rate of comparably supported catalysts reported in the literature were about one order of magnitude lower than the rate of methanol synthesis. Among the tested catalysts, $Pd_5Y_{95}O_x$ was the most selective catalyst for temperatures above 265 °C.

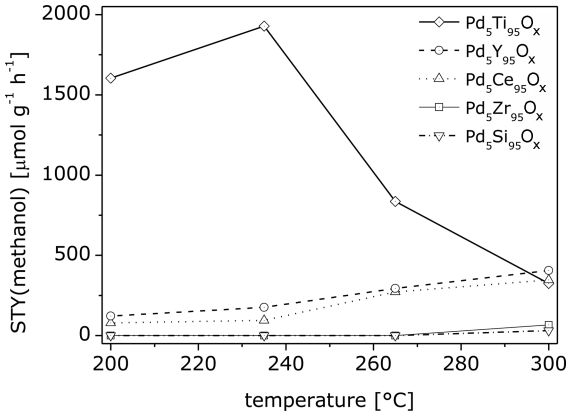

Figure 5. Comparison of the space time yields of methanol for the catalysts of generation 1. Reaction conditions: P = 30 bar; total flow rate: 12 mL/min (CO/H_2 = 33/67); catalyst weight: 100 mg (50−100 μm) diluted with 400 mg quartz sand (100−200 μm); WHSV = 12.

Results of Generation 2. Since in the first generation no catalyst with both high activity and high selectivity toward methanol could be identified, it was the objective of the second generation to improve the reactivity behavior by doping and combining of matrix elements. All catalysts were tested in the 10-channel microreactor at 30 bar pressure. The general composition of the catalysts of this generation was $Pd_5M^1{}_{10}M^2{}_{85}O_x$, where M^2 denotes the matrix element and M^1 the dopant. Cr and Al were chosen in addition to the same elements as in generation 1 for M^1. Although these elements did not yield gelating precursors in the synthesis method applied here, they could be used as dopants in combination with the matrix oxides. The methanol yields of the second generation relative to the yield of the reference catalyst are given in Figure 6. The most active catalysts were of the group of

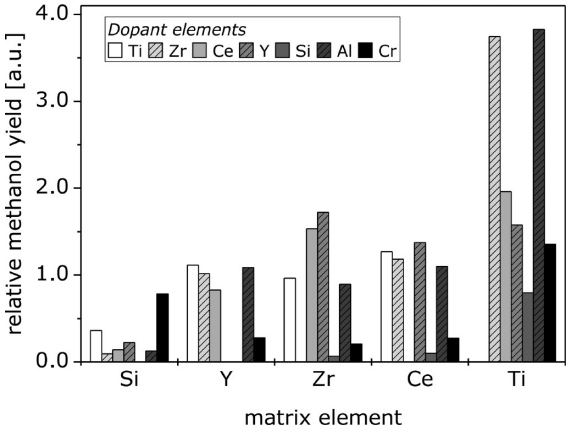

Figure 6. Relative methanol production of generation 2 (normalized to methanol yield of $Cu/ZnO/Al_2O_3$). Testing conditions: P = 30 bar; T = 235 °C; total flow rate: 12 mL/min; measurement time per sample: 4.5 h.

dx.doi.org/10.1021/co200191a | ACS Comb. Sci. 2012, 14, 378−387

Ti-based catalysts. The Si-based catalysts, on the other hand, showed the lowest activities. These findings were in good agreement with the trends found in the first generation. As can be seen in Figure 6 the activity of the catalysts depended strongly on the dopant element. However, no clear correlation between dopant and activity could be deduced. Generally Ti, Zr, and Al seemed to have an activating effect while Si had a deactivating effect. The biggest differences were found for Y: While the Ti-based catalysts were deactivated upon doping with Y, $Pd_5Y_{10}Zr_{85}O_x$ and $Pd_5Y_{10}Ce_{85}O_x$ were the most active catalysts in the group of doped Zr- and Ce-based catalysts, respectively. As $Pd_5Zr_{10}Y_{85}O_x$ was among the most active catalyst materials, it seemed likely, that the formation of a Y-stabilized ZrO_2 phase was favorable for methanol synthesis. The doping of the catalytically inactive materials $Pd_5Si_{95}O_x$ and $Pd_5Zr_{95}O_x$ resulted always in an activation, independent of the dopant. As the activity trends of the dopant elements were in agreement with the trends observed for the corresponding oxides in the first generation, the gain in catalytic activity could obviously be ascribed to the intrinsic catalytic activity of the dopant elements.

The strong dopant effects observed in the screening were confirmed in the conventional catalytic tests. Among the group of Ti-based catalysts, as can be seen in Table 1, $Pd_5Zr_{10}Ti_{85}O_x$ and $Pd_5Cr_{10}Ti_{85}O_x$ showed methanol yields above 1500 μmol g^{-1} h^{-1} at 200 °C, while the other catalysts exhibited only moderate methanol yields lower than 500 μmol g^{-1} h^{-1}. However, all doped catalysts showed lower space time yields than undoped $Pd_5Ti_{95}O_x$. The conventional tests also revealed that the competitive methanation reaction was much more composition sensitive than the methanol formation.

Table 1. Results of the Catalytic Tests of the Ti Based Catalysts[a]

		STY (methanol)	STY (methane)
		(μmol g^{-1} h^{-1})	
$Pd_5Ti_{95}O_x$	200 °C	1604	116
	235 °C	1928	803
$Pd_5Zr_{10}Ti_{85}O_x$	200 °C	1510	242
	235 °C	1968	1231
$Pd_5Cr_{10}Ti_{85}O_x$	200 °C	1100	267
	235 °C	1850	1180
$Pd_5Ce_{10}Ti_{85}O_x$	200 °C	463	203
	235 °C	670	784
$Pd_5Y_{10}Ti_{85}O_x$	200 °C	367	287
	235 °C	437	1195
$Pd_5Al_{10}Ti_{85}O_x$	200 °C	157	44
	235 °C	762	585
$Pd_5Si_{10}Ti_{85}O_x$	200 °C	59	145
	235 °C	215	740

[a]Reaction conditions: P = 30 bar; total flow rate: 12 mL/min (CO/H_2 = 33/67); catalyst weight: 100 mg (50−100 μm) diluted with 400 mg of quartz sand (100−200 μm); WHSV = 12.

The Ce-based catalysts showed the highest methanol selectivities, and the methanation reaction was influenced to a much smaller extent by doping than the Ti-based catalysts. In contrast to the other catalysts, the methanol synthesis reaction was strongly influenced by the doping. In Figures 7(c) and (d) it can be seen that by doping with 10 mol% Zr, the methanol yield was enhanced by a factor of almost 20, while the methanation reaction was only accelerated by a factor of 2.

The space time yields of methanol and methane for the Zr based catalysts are given in Figures 7(a) and (b). By Y doping the methanol yield was remarkably increased; however, a comparably poor selectivity was achieved because of high methanation rates.

Results of Generation 3. Although $Pd_5Zr_{10}Ce_{85}O_x$ and $Pd_5Y_{10}Zr_{85}O_x$ showed promising space time yields of methanol, no catalyst of generation 2 showed as high methanol yields as $Pd_5Ti_{95}O_x$. It has been shown that the doping with transition metals affected mainly the methanation reaction.[13] Since a promoting effect of alkaline and earth alkaline metals on supported Pd catalysts has already been observed,[13,35] it was the aim of the third generation to investigate the influence of alkaline and alkaline earth metal doping on methanol formation. The oxides were doped in concentrations of 1 and 3 mol%, while the Pd content was varied between 3 and 5 mol %. The results of the screening are presented in Figure 8. It is clearly seen that alkaline earth metals had a stronger promoting effect than alkaline metals, where the highest methanol yield was obtained by Mg doping.

The results of the screening were confirmed by conventional testing. Only $Rb_3Pd_5Ti_{92}O_x$ was identified as a "false positive". The promoting effect of the earth alkaline metals decreased with increasing atomic mass within the group. The methanol yields of the Mg doped catalysts are given in Figure 9. It can be seen that the concentration of the dopant has a strong influence on the catalytic activity: While 1 mol% Mg promotes the reaction, a content of 3 mol% has an inhibiting effect. This was in contradiction to the screening results where the doping with 3 mol% Mg did result in higher methanol yields than the doping with 1 mol%. All alkaline earth metals accelerated the methanation so that only poor methanol selectivities were achieved. It was concluded that apart from the Mg-doping no remarkable improvement of $Pd_5Ti_{95}O_x$ was achieved by doping in generation 3.

Results of Generation 4. The fourth generation was based on the results of generations 2 and 3. Ti was kept as matrix element, while Al, Si, Cr, and Zr were chosen as dopants (Dot). The catalysts of generation 4 were of the general composition $Mg_yPd_5Dot_{10}Ti_{85-y}O_x$. From the screening results, which are given in Figure 10, no clear trends on the role of the dopants could be drawn. All materials were less active than $Pd_5Ti_{95}O_x$ and $Mg_1Pd_5Ti_{94}O_x$. At this point the screening process was aborted. In Fig. 11 the performance of the mixed oxide $Pd_5Ti_{95}O_x$ is compared with a Pd-impregnated TiO_2 of identical composition. It documents the improved performance of the mixed oxide.

3.2. Characterization. To elucidate the influence of different dopant elements on the catalytic reactivity of the materials studied, the structure and morphology of the catalyst system Mg−Pd−Cr−Ti ($Pd_5Ti_{95}O_x$, $Mg_1Pd_5Ti_{94}O_x$, $Pd_5Cr_{10}Ti_{85}O_x$, $Mg_1Pd_5Cr_{10}Ti_{84}O_x$) which showed a large variety of different methanol yields was investigated by several techniques. Additionally, $Pd_5Zr_{10}Ce_{85}O_x$ and $Pd_5Y_{10}Zr_{85}O_x$ were characterized as well, as they showed good activities and selectivities for methanol synthesis during the screening.

All sol−gel materials were characterized by high specific surface areas (SSA) in the order of 200−300 m^2/g. The surface area and pore structure of these materials was strongly influenced by the dopant elements, as can be seen from Table 2. While the doping with Mg resulted in a slight increase of the pore volume, the pore volume drastically decreased upon Cr doping. By doping with both Cr and Mg, the highest SSA

dx.doi.org/10.1021/co200191a | ACS Comb. Sci. 2012, 14, 378−387

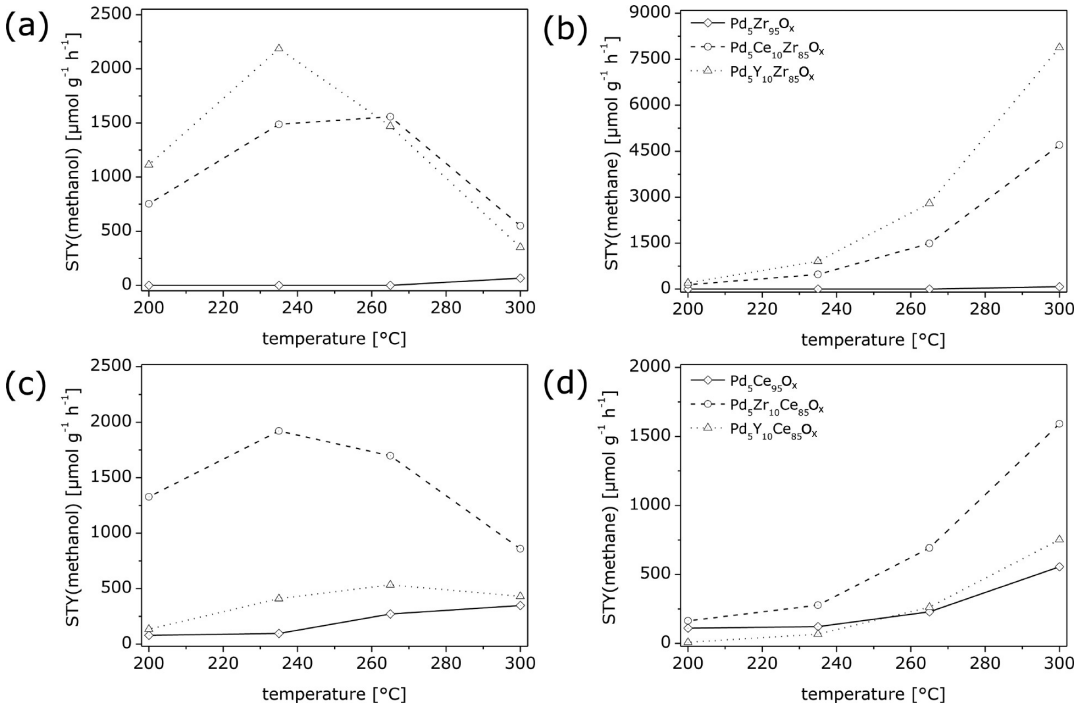

Figure 7. Results of the catalytic tests of the Ce and Zr based catalysts. Reaction conditions: P = 30 bar; total flow rate: 12 mL/min (CO/H_2 = 33/67); catalyst weight: 100 mg (50−100 μm) diluted with 400 mg quartz sand (100−200 μm); WHSV = 12.

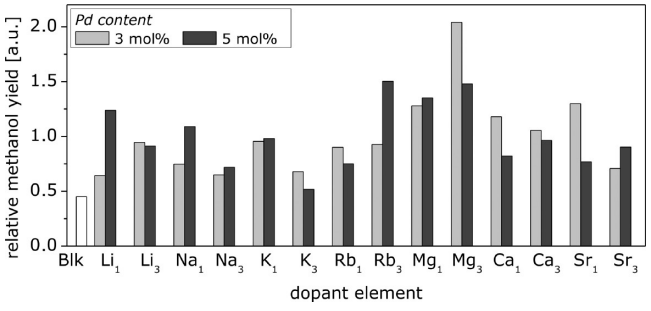

Figure 8. Relative methanol production of generation 3 catalysts $Dot_zPd_yTi_{95-z-y}O_x$ (normalized to methanol yield of $Cu/ZnO/Al_2O_3$). Testing conditions: P = 30 bar; T = 235 °C; total flow rate: 12 mL/min; measurement time per sample: 4.5 h.

and pore volume among the considered catalysts were achieved, which might be an indication for a possible synergistic dopant effect of the two metals.

The N_2 adsorption isotherms of all materials were characterized by a steep increase of the adsorbed volume in the low pressure region (p/p^0 < 0,1), which could be an indication for the presence of micropores ($d_P \leq 2$ nm). Micropores in nonzeolitic materials are rare and of general interest. Clear evidence for microporosity is an inflection point at $10^{-5} \leq p/p^0 \leq 10^{-1}$ in the logarithmic representation of the Ar adsorption isotherm.[36] Therefore Ar adsorption isotherms were obtained at the temperature of liquid Ar (87.5 K), but the absence of an inflection point at low pressure for all samples documents the absence of micropores. The results are summarized in Table 2 (the Ar-based data are nearly identical to those obtained with N_2 adsorption isotherms (not shown)).

The catalysts were investigated by powder X-ray diffraction in the prepared as well as in the reduced state. The broad peaks

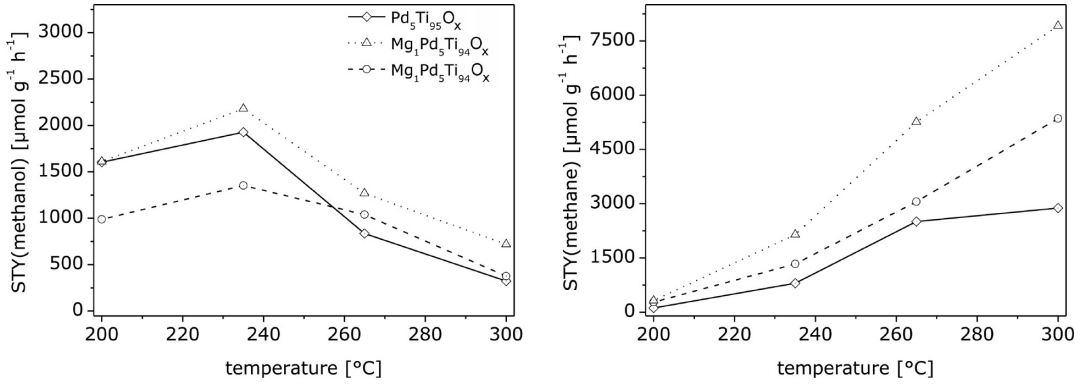

Figure 9. Results of the catalytic tests of the Mg doped Ti-based catalysts. Reaction conditions: P = 30 bar; total flow rate: 12 mL/min (CO/H_2 = 33/67); catalyst weight: 100 mg (50−100 μm) diluted with 400 mg of quartz sand (100−200 μm); WHSV = 12.

dx.doi.org/10.1021/co200191a | ACS Comb. Sci. 2012, 14, 378−387

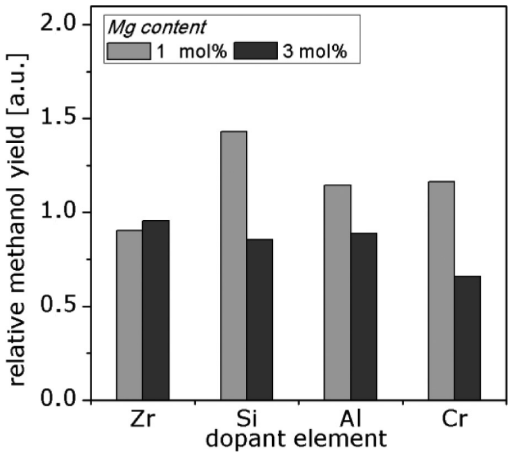

Figure 10. Relative methanol production of generation 4 catalysts $Mg_zPd_5Dot_{10}Ti_{85-z}O_x$. (normalized to methanol yield of Cu/ZnO/Al_2O_3) Testing conditions: P = 30 bar; T = 235 °C; total flow rate: 12 mL/min; measurement time per sample: 4.5 h.

Table 2. Overview on Structural Properties of Various Pd Based Mixed Oxides Obtained by Ar Physisorption at T = 87.5 K

	S_{BET}	V_{pore}	pore radius distribution	
	(m^2/g)	(cm^3/g)	maximum pore radius (nm)	median pore radius (nm)
$Pd_5Ti_{95}O_x$	250	0.135	1.29	1.73
$Mg_1Pd_5Ti_{94}O_x$	258	0.146	1.30	1.66
$Pd_5Cr_{10}Ti_{85}O_x$	202	0.111	1.26	1.65
$Mg_1Pd_5Cr_{10}Ti_{84}O_x$	272	0.145	1.23	1.58
$Pd_5Zr_{10}Ce_{85}O_x$	95	0.076	1.29	3.53
$Pd_5Y_{10}Zr_{85}O_x$	191	0.143	1.23	2.06
$Pd_5Zr_{95}O_x$	12	0.009	1.29	3.50

in the diffraction patterns for the Ti-based materials given in Figure 12 indicated that the sol–gel materials show a small crystallite size with the possibility of amorphous fractions, which made an analysis difficult because of overlapping reflections. The phase analysis of the Ti-based materials revealed anatase, palladinite (PdO), and Pd as the only observable crystalline phases. This indicated that Mg and Cr were either present in an amorphous state in the mixed oxide or were substituted into the lattices of the crystalline phases. The exchange of Ti^{4+} by Cr^{3+} in the anatase crystal lattice was reported in numerous studies.[37−39] Furthermore, the anatase structure offers interstitial sites which could be occupied by small ions such as Mg^{2+}.[40] The doping influenced the crystallization of both the Pd and Ti containing fractions. On the basis of intensity and peak broadening of anatase in $Pd_5Cr_{10}Ti_{85}O_x$, it can be concluded that Cr inhibits the crystallization. This is in good agreement with results by Khaleel et al. who showed that Cr doping inhibited the crystallization of TiO_2 phases.[41] Mg seemed to support the crystallization of PdO as can be seen from the pronounced palladinite diffraction patterns observed for $Mg_1Pd_5Ti_{94}O_x$ and $Mg_1Pd_5Cr_{10}Ti_{84}O_x$. During the reductive pretreatment, a crystallization and crystal growth of TiO_2 took place, which could be seen from the growth in intensity of the anatase diffraction peaks. As for the doped catalysts, lower intensities of the anatase reflections were observed after reduction, the dopants seemed to have a stabilizing effect on the amorphous matrix by inhibiting crystallization upon reduction.

Rietveld analysis of the lattice parameters revealed that the anatase unit cell parameters were significantly decreased in the as-prepared state. Upon reduction, the unit cell expanded (see Table 3). As this effect was observed for all materials, this phenomenon might be explained by the insertion of Pd^{2+} into the anatase lattice. As the ionic radii of Ti^{4+} for CN = 6 (0.605 Å[42]) and Pd^{2+} (0.86 Å [42]) are quite different and the Pd^{2+} radius exceeds the radii ratio limit of an octahedral coordination ($0.414 \leq r_c/r_a \leq 0.528$ with r_a = 1.40 Å), substitution only at interstitial positions seems reasonable. For charge neutrality reasons, each Ti^{4+} has to be replaced either by two Pd^{2+} ($Pd_{2x}Ti_{1-x}O_2$) or by one Pd^{2+} and generation of an additional O^{2-} vacancy ($Pd_xTi_{1-x}O_{2-x}$). Crişan et al. showed that a Pd content of 0.5 and 1 wt % resulted in a decreased unit cell.[43] Although no definite evidence could be given, it is highly probable that a small amount of Pd^{2+}—but also a small amount of other doping cations—was incorporated into the TiO_2 lattice resulting in the contraction of the unit cell. Unit cell expansion upon reduction is another hint that Pd^{2+} is effectively incorporated into the TiO_2 lattice and removed when reduced to metallic Pd.

While the doping of $Pd_5Ti_{95}O_x$ inhibited the crystallization of the matrix, the opposite effect is observed for Y doping of $Pd_5Zr_{95}O_x$. $Pd_5Zr_{95}O_x$ was completely amorphous, while the crystalline phases palladinite and tetragonal ZrO_2 were present in $Pd_5Y_{10}Zr_{85}O_x$, as can be seen in Figure 13. The stabilizing effect of Y on tetragonal ZrO_2 is well-known and widely

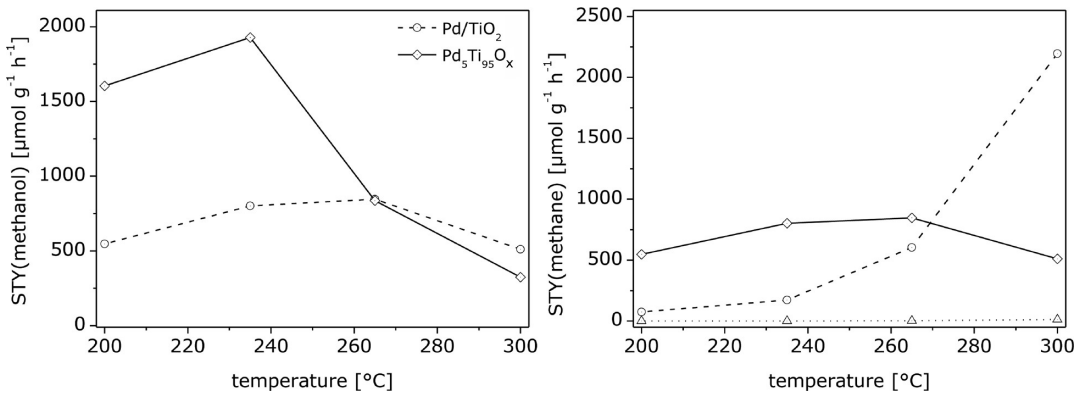

Figure 11. Comparison of catalytic performances of $Pd_5Ti_{95}O_x$ and Pd/TiO_2. Reaction conditions: P = 30 bar; total flow rate: 12 mL/min (CO/H_2 = 33/67); catalyst weight: 100 mg (50−100 μm) diluted with 400 mg of quartz sand (100−200 μm); WHSV = 12.

dx.doi.org/10.1021/co200191a | ACS Comb. Sci. 2012, 14, 378−387

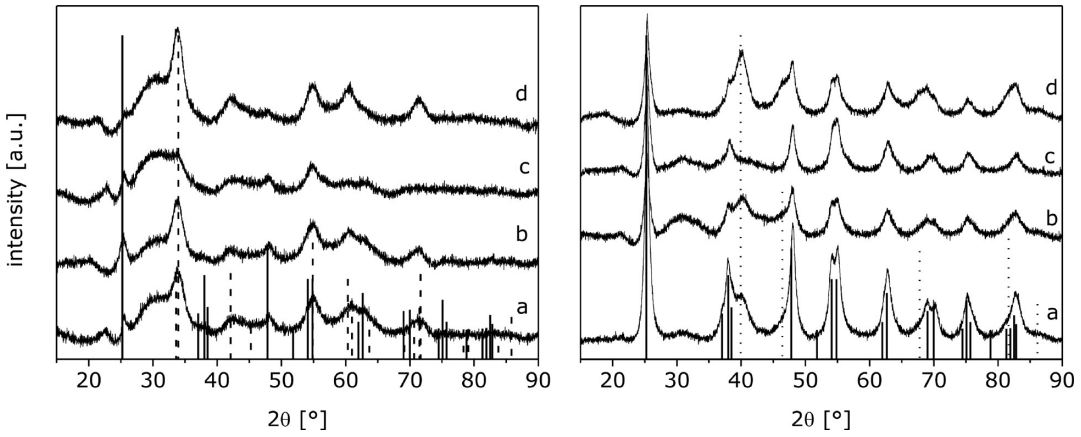

Figure 12. Powder XRD patterns of $Pd_5Ti_{95}O_x$ (a), $Mg_1Pd_5Ti_{94}O_x$ (b), $Pd_5Cr_{10}Ti_{85}O_x$ (c), $Mg_1Pd_5Cr_{10}Ti_{84}O_x$ (d); *left:* as prepared; *right:* after reductive pretreatment. Solid lines, anatase (TiO_2, ICSD: 154610); dotted lines, Pd (ICSD: 64920); dashed lines, palladinite (PdO, ICSD: 29281).

Table 3. Summary of the Structural Parameters of the Crystalline Parts of the Ti Based Materials[a]

		as prepared		activated[b]	
		PdO	TiO_2	Pd	TiO_2
$Pd_5Ti_{95}O_x$	*a* (Å)	3.030(2)	3.765(2)	3.888(1)	3.7847(4)
	c (Å)	5.296(6)	9.425(7)		9.471(1)
	D (nm)	4.5(1)	11(1)	4.0(1)	11.9(1)
$Mg_1Pd_5Ti_{94}O_x$	*a* (Å)	3.035(2)	3.769(2)	3.887(1)	3.784(1)
	c (Å)	5.307(6)	9.444(8)		9.461(3)
	D (nm)	4.9(1)	7.5(3)	3.9(1)	10.7(2)
$Pd_5Cr_{10}Ti_{85}O_x$	*a* (Å)	*c*	*c*	3.879(4)	3.789(1)
	c (Å)	*c*	*c*		9.435(2)
	D (nm)	*c*	*c*	8(1)	11.4(2)
$Mg_1Pd_5Cr_{10}Ti_{84}O_x$	*a* (Å)	3.033(1)	3.778(4)	3.900(1)	3.790(1)
	c (Å)	5.317(5)	9.43(2)		9.461(3)
	D (nm)	5.7(2)	15(2)	4.3(1)	10

[a]The standard deviations of the last indicated digit are given in parentheses. *a*,*c*: lattice parameters; *D*: crystallite size. [b]Two hours in 50% H_2 in N_2 at 300 °C. [c]No analysis possible because of low crystallinity of the sample.

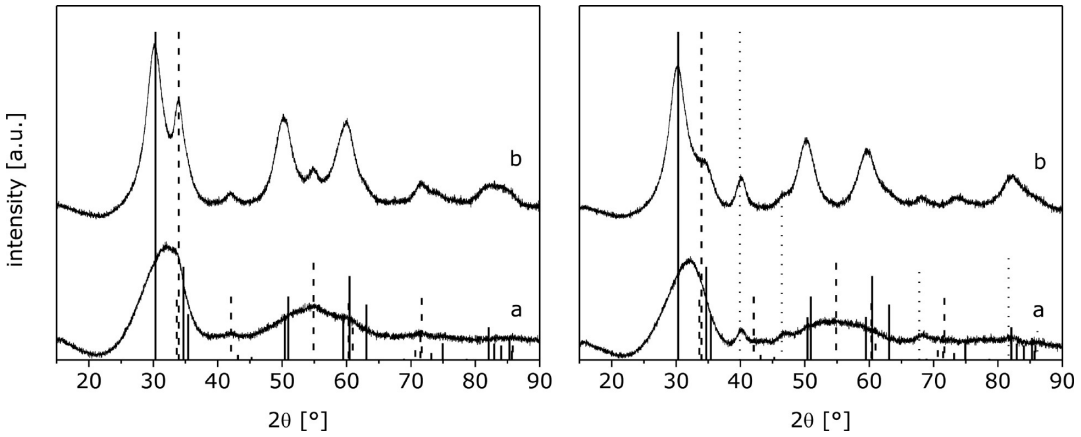

Figure 13. Powder XRD patterns of $Pd_5Zr_{95}O_x$ (a), $Pd_5Y_{10}Zr_{85}O_x$ (b); *left:* as prepared; *right:* after reductive pretreatment. Solid lines, ZrO_2 (tetragonal, ICSD: 66781); dotted lines, Pd (ICSD: 64920); dashed lines, palladinite (PdO, ICSD: 29281).

described in literature.[44,45] It is noteworthy that the catalytic activity is a result of the structuring of the material. The shoulder at 2Θ = 35° of reduced $Pd_5Y_{10}Zr_{85}O_x$ indicates incomplete reduction of Pd resulting in the necessity to include PdO in the Rietveld refinement of the diffraction data to achieve best refinement results. Since cationic Pd species are believed to be active centers in methanol synthesis, this could be an explanation for the extraordinary catalytic properties of $Pd_5Y_{10}Zr_{85}O_x$.

For the highly selective catalyst $Pd_5Zr_{10}Ce_{85}O_x$ no crystalline Pd phases could be observed neither in the as-prepared nor in the reduced state indicating a high dispersion of Pd. Since the incorporation of Pd into the CeO_2 lattice is in general possible,[46] this could be another explanation for the absence of

dx.doi.org/10.1021/co200191a | *ACS Comb. Sci.* 2012, 14, 378–387

crystalline Pd phases. Rietveld analysis of the crystalline CeO_2 phase showed a slightly decreased unit cell parameter, which could be the result of the incorporation of Zr^{4+} into the lattice.[47] Nevertheless, it should be emphasized, that all materials shown in Figure 12 and 13 are most likely nanocrystals embedded in a highly amorphous matrix. This highly amorphous nature is also the reason why structural characterization of the prepared mixed oxides is limited. TEM analysis has therefore been restricted to $Pd_5Ti_{95}O_x$, which is most likely representative for the microstructure of all the materials of Figures 12 and 13.

The TEM analysis of $Pd_5Ti_{95}O_x$ (see Figure 14) confirmed the dominating amorphous nature of the mixed oxide; it

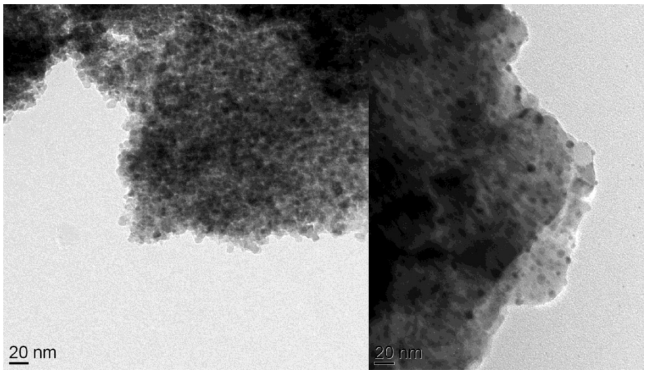

Figure 14. TEM images of as-prepared (left) and activated (right) $Pd_5Ti_{95}O_x$.

showed agglomerations of about 10 nm large particles with a homogeneous distribution of Pd and Ti. Isolated particles of PdO could be observed in highly resolved images. The particle sizes concurred with those determined from peak broadening of the X-ray diffraction patterns. The reductive activation resulted in the formation of metallic Pd particles. From HRTEM imaging a decoration of Pd by the TiO_2 matrix could be deduced, which is a good indication for the presence of strong metal support interactions between Pd and Ti. EDX mapping (not shown) confirmed the composition (5% Pd, 95% Ti) over the areas studied.

The results of the characterization can be summarized as follows.

Via the here presented sol−gel synthesis route Pd containing mixed oxides with high specific surface area and large pore volumes are accessible. XRD data indicate small particle sizes and significant amorphous character. TEM analysis revealed that $Pd_5Ti_{95}O_x$ consisted of small particles in the scale of few nanometers, which showed a homogeneous distribution of the elements (based on EDX). During reduction a demixing of the elements took place to a certain degree resulting in with the formation of Pd particles with a narrow particle size distribution.

Although the doping elements had a strong influence on the reactivity of the catalysts, no clear relationship between reactivity and structural properties could be derived. It appeared that Mg influenced mainly the crystallization of Pd. As only small morphological changes were observable, a minute modification of the chemical nature of the active center in such a way that CO dissociation was favored over nondissociative hydrogenation is more probable. Cr, on the other hand, seemed to have an influence on TiO_2 as could be seen from the lower degree of crystallinity of anatase for the Cr doped catalysts. In general Cr doping resulted in lower methanol yields; however, no correlation between crystallinity and methanol synthesis activity could be deduced.

The addition of Y to $Pd_5Zr_{95}O_x$ resulted in a highly active catalyst with a high specific surface area and large pore volume. The crystallization of ZrO_2 is enhanced by Y_2O_3, which is in good agreement with the well-known stabilizing effect of Y_2O_3 on ZrO_2.

The best methanol selectivity was observed for $Pd_5Zr_{10}Ce_{85}O_x$. Since this catalyst did neither exhibit a high surface area nor a large pore volume among the considered catalysts, it seemed that these are not necessary requirements for the catalytic properties of $Pd_5Zr_{10}Ce_{85}O_x$. A more likely explanation might be the high Pd dispersion.

4. CONCLUSION

Novel Pd based mixed oxides were synthesized by the sol−gel method. In a combinatorial approach these materials were screened for their catalytic methanol synthesis activity. For the screening a microstructured reactor was used, which allowed for the sequential testing of up to 10 catalysts at 30 bar pressure. As can be seen in Figure 11 higher methanol yields were achieved in comparison to analogous supported catalysts. Although all catalysts showed significant activity for methanation, which increased strongly with temperature, Pd containing homogeneously mixed oxides showed to be a promising class of catalysts for methanol synthesis. Besides $Pd_5Ti_{95}O_x$, $Pd_5Y_{10}Zr_{85}O_x$, and $Pd_5Zr_{10}Ce_{85}O_x$ were identified as promising new catalysts. While the highest space time yield of methanol was achieved for $Pd_5Ti_{95}O_x$, $Pd_5Zr_{10}Ce_{85}O_x$ showed the best selectivity toward methanol. In general, these catalysts exhibited good selectivities between 200 and 235 °C.

To investigate the influence of different dopant elements, $Mg_1Pd_5Ti_{94}O_x$, $Pd_5Cr_{10}Ti_{85}O_x$, and $Mg_1Pd_5Cr_{10}Ti_{84}O_x$ were characterized and compared to $Pd_5Ti_{95}O_x$. Whereas the methanol synthesis remained almost unaffected, the side reaction to methane was strongly promoted by the dopants. As the materials remained partly amorphous, the role of the single dopants remains uncertain.

AUTHOR INFORMATION

Corresponding Author

*Phone: (+49)681-302-2582. Fax: 0049-(0)681-302-2343. E-mail: w.f.maier@mx.uni-saarland.de.

Notes

The authors declare no competing financial interest.

ACKNOWLEDGMENTS

The authors thank BASF-SE for the donation of the Cu−Zn reference catalyst.

REFERENCES

(1) Cheng, W.-H.; Kung, H. H. *Methanol Production and Use*; Marcel Dekker: New York, 1994.

(2) Floren, J. A. Successful Global Industry Depends on Open Markets. *Methanol Institute Milestones*, 2010.

(3) Olah, G.; Goepert, A.; Prakash, G. *Beyond oil and gas: the methanol economy*; Wiley-VCH: Weinheim, Germany, 2006.

(4) Spencer, M. S. The role of zinc oxide in Cu/ZnO catalysts for methanol synthesis and the water-gas shift reaction. *Top. Catal.* **1999**, *8*, 259−266.

(5) Ward, A.; Bruni, E.; Lykkegaard, M.; Feilberg, A.; Adamsen, A.; Jensen, A.; Poulsen, A. Real time monitoring of a biogas digester with gas chromatography, near infrared spectroscopy, and membrane-inlet mass spectrometry. *Bioresour. Technol.* **2011**, *102*, 4098−4103.
(6) Poutsma, M. L.; Elek, L. F.; Ibarbia, P. A.; Risch, A. P.; Rabo, J. A. Selective formation of methanol from synthesis gas over palladium catalysts. *J. Catal.* **1978**, *52*, 157−168.
(7) Ryndin, Y.; Hicks, R.; Bell, A.; Yermakov, Y. Effects of metal-support interactions on the synthesis of methanol over palladium. *J. Catal.* **1981**, *70*, 287−297.
(8) Fajula, F.; Anthony, R.; Lunsford, J. Methane and methanol synthesis over supported palladium catalysts. *J. Catal.* **1982**, *73*, 237−256.
(9) Shen, W.-J.; Okumura, M.; Matsumura, Y.; Haruta, M. The influence of the support on the activity and selectivity of Pd in CO hydrogenation. *Appl. Catal., A* **2001**, *213*, 225−232.
(10) Ponec, V. Cu and Pd, two catalysts for CH_3OH synthesis: the similarities and the differences. *Surf. Sci.* **1992**, *272*, 111−117.
(11) Ponec, V. Active centres for synthesis gas reactions. *Catal. Today* **1992**, *12*, 227−254.
(12) Berlowitz, P.; Goodman, D. The activity of Pd(110) for methanol synthesis. *J. Catal.* **1987**, *108*, 364−368.
(13) Driessen, J.; Poels, E.; Hinderman, J.; Ponec, V. On the selectivity of palladium catalysts in synthesis gas reactions. *J. Catal.* **1983**, *82*, 26−34.
(14) Sellmer, C.; Prins, R.; Kruse, N. XPS/SIMS studies of the promoter action in methanol synthesis over silica-supported Pd catalysts. *Catal. Lett.* **1997**, *47*, 83−89.
(15) Gotti, A.; Prins, R. Basic metal oxides as co-catalysts in the conversion of synthesis gas to methanol on supported palladium catalysts. *J. Catal.* **1998**, *175*, 302−311.
(16) Gusovius, A.; Watling, T.; Prins, R. Ca promoted Pd/SiO_2 catalysts for the synthesis of methanol from CO: the location of the promoter. *Appl. Catal., A* **1999**, *188*, 187−199.
(17) Matsumura, Y.; Shen, W.-J.; Ichihashi, Y.; Okumura, M. Low-temperature methanol synthesis catalyzed over ultrafine palladium particles supported on cerium oxide. *J. Catal.* **2001**, *197*, 267−272.
(18) Shen, W.; Ichihashi, Y.; Matsumura, Y. A comparative study of palladium and copper catalysts in methanol synthesis. *Catal. Lett.* **2002**, *79*, 125−127.
(19) Badri, A.; Binet, C.; Lavalley, J.-C. Metal-support interaction between Pd/CeO_2 catalysts. *J. Chem. Soc., Faraday Trans.* **1996**, *92*, 1603−1608.
(20) Ma, Y.; Ge, Q.; Li, W.; Xu, H. Methanol synthesis from sulfur-containing syngas over Pd/CeO_2 catalyst. *Appl. Catal., B* **2009**, *90*, 99−104.
(21) Maier, W. F.; Stöwe, K.; Sieg, S. C. Kombinatorische und Hochdurchsatz-Techniken in der Materialforschung. *Angew. Chem.* **2007**, *119*, 6122−6179.
(22) Frenzer, G.; Maier, W. F. Amorphous porous mixed oxides: sol-gel ways to a highly versatile class of materials and catalysts. *Annu. Rev. Mater. Res.* **2006**, *36*, 281−331.
(23) Kim, D. K. Combinatorial and conventional development of new catalysts for the CO_2 reforming of methane. Ph.D. Thesis, Universität des Saarlandes, Saarbrücken, Germany, 2006.
(24) Brunauer, S.; Emmett, P.; Teller, E. Adsorption of gases in in multimolecular layers. *J. Am. Chem. Soc.* **1938**, *60*, 309.
(25) Fagerlund, G. Determination of specific surface by the BET method. *Mater.Constr.* **1973**, *6*, 239.
(26) Barrett, E.; Joyner, L.; Halenda, P. The determination of pore volume and area distributions in porous substances. I. Computations from nitrogen isotherms. *J. Am. Chem. Soc.* **1951**, *73*, 373.
(27) *X'Pert HighScore Plus, Complete Full Powder Pattern Analysis Tool*, v2.2c; PANalytical B.V., Almelo, The Netherlands, 2007.
(28) *TOPAS, General Profile and Structure Analysis Software of Powder Diffraction Data*, v2.1; Bruker AXS: Karlsruhe, Germany, 2003.
(29) Weiss, T. Entwicklung neuer heterogener Katalysatoren zur Spaltung von Methanol in Wasserstoff und Kohlenmonoxid mittels Hochdurchsatz-Methoden. Ph.D. Thesis, Universität des Saarlandes, Saarbrücken, Germany, 2008.
(30) Reiser, M. Inbetriebnahme und Einrichtung eines Parallel-Mikrostrukturreaktors für die Anwendung in Hochdurchsatz-Screeningexperimenten in der heterogenen Katalyse. Diploma Thesis, Universität des Saarlandes, Saarbrücken, Germany, 2007.
(31) Schüth, F.; Hoffmann, C.; Wolf, A.; Schunk, S.; Stichert, W.; Brenner, A. High-througput experimentation in catalysis. In *Combinatorial chemistry: synthesis, analysis, screening*; Jung, G., Ed.; Wiley-VCH: Weinheim, Germany, 1999; pp 463−477.
(32) Borgschulte, A.; Westerwaal, R.; Rector, J.; Dam, B.; Griessen, R.; Schoenes, J. Effect of strong metal-support interactions on hydrogen sorption kinetics of Pd-capped switchable mirrors. *Phys. Rev. B* **2004**, *70*, 155414.
(33) Vannice, M. The catalytic synthesis of hydrocarbons form H_2/CO misture over the group VII metal. I. The specific activities and product distributions of supported metlas. *J. Catal.* **1975**, *37*, 449−461.
(34) Vannice, M. The catalytic synthesis of hydrocarbons form H_2/CO misture over the group VII metal. II. The kinetics of the methanation reaction over supported metals. *J. Catal.* **1975**, *37*, 462−273.
(35) Gotti, A.; Prins, R. Effect of metal oxide additives on the CO hydrogenation to methanol over Rh/SiO_2 and Pd/SiO_2. *Catal. Lett.* **1996**, *37*, 143−151.
(36) Storck, S.; Bretinger, H.; Maier, W. F. Characterization of micro- and mesoporous solids by physisorption methods and pore-size analysis. *Appl. Catal., A* **1998**, *174*, 137−146.
(37) Ranjit, K.; Viswanathan, B. Photocatalytic reduction of nitrite and nitrate ions over doped TiO_2 catalysts. *J. Photochem. Photobiol.* **1997**, *107*, 215−220.
(38) Wilke, K.; Breuer, H. The influence of transition metal doping on the physical and photocatalytical properties of titania. *J. Photochem. Photobiol.* **1999**, *121*, 49−53.
(39) Kaspar, T.; Droubay, T.; Shutthanandan, V.; Heald, S.; Wang, C.; McCready, D.; Thevuthasan, S.; Bryan, J.; Gamelin, D.; Kellock, A.; Toney, M.; Hong, X.; Ahn, C.; Chambers, S. Ferromagnetism and structure of epitaxial Cr-doped anatase TiO_2 thin films. *Phys. Rev. B* **2006**, *73*, 155327.
(40) Shirley, R.; Kraft, M.; Inderwildi, O. Electronic and optical properties of aluminum-doped anatase and rutile TiO_2 from *ab initio* calculations. *Phys. Rev. B* **2010**, *81*, 075111.
(41) Khaleel, A.; Shehadi, I.; Al-Shamisi, M. Structural and textural characerization of sol-gel prepared nano scale titanium-chromium mixed oxides. *J. Non-Cryst. Solids* **2010**, *356*, 1282−1287.
(42) Shannon, R. D. Revised effective ionic radii and systematic studies of interatomic distances in halides and chalcogenides. *Acta Crystallogr., Sect. A* **1976**, *32*, 751−767.
(43) Crişan, D.; Drăgan, N.; Crişan, M.; Răileanu, M.; Brăilenu, A.; Anastasescu, M.; Ianculesu, A.; Mardare, D.; Luca, S.; Marinescu, V.; Moldovan, A. Crystallization study of sol-gel doped un-doped and Pd-doped TiO_2 materials. *J. Phys. Chem. Solids* **2008**, *69*, 2548−2554.
(44) Jebrouni, M.; Durand, B.; Roubin, M. Preparation of yttrium stabilized zirconia by reaction in molten nitrates and characterization. *Ann. Chim.* **1992**, *17*, 143−154.
(45) Borik, M.; Vishnyakova, W.; Kulebyakin, A.; Lomonova, E.; Myzina, V.; Osiko, V.; Panov, V. Preparation and properties of Y_2O_3 partially stabilized ZrO_2 crystals. *Inorg. Mater.* **2007**, *43*, 1223−1229.
(46) Yang, Z.; Luo, G.; Lu, Z.; Hermansson, K. Oxygen vacancy formation energy in Pd-doped ceria: a DFT+U study. *J. Chem. Phys.* **2007**, *127*, 074704.
(47) Jen, H.-W.; Graham, G.; Chun, W.; McCabe, R.; Cuif, J.-P.; Deutsch, S.; Touret, O. Characterization of model exhaust catalysts: Pd on ceria and ceria-zirconia supports. *Catal. Today* **1999**, *50*, 309−328.